Multiphoton Lithography of Unconstrained Three-Dimensional Protein Microstructures

*Eric C. Spivey, Eric T. Ritschdorff, Jodi L. Connell, Christopher A. McLennon, Christine E. Schmidt, and Jason B. Shear**

Multiphoton lithography (MPL) is a highly versatile strategy for creating 3D microscale objects with complex geometrical arrangements, including nested boxes, interlocking blocks, and braided threads. Of the various chemistries used to produce solid forms in MPL, protein photocrosslinking has been of particular value in biological applications, yielding materials with high porosity, tunable elasticity, and a diverse set of chemical and biochemical properties. Unfortunately, the potential for object drift, and consequent distortion, during this direct-write process has required that microforms be constructed in integral contact with an immobile surface, precluding fabrication of protein-based objects that retain rotational and translational degrees of freedom. Here, the development of a high-viscosity protein-based reagent that can be used to fabricate complex 3D microstructures that are not adhered to a surface, including chains of Möbius strips, paddlewheels, and unconstrained (free-floating) probes for bacterial motility, is reported.

1. Introduction

Although lithographic techniques exist for producing microscale features within a broad range of materials, nearly all lack the ability to precisely control 3D morphology.[1,2] To address this need, various investigators have explored microfabrication using multiphoton lithography (MPL), a direct-write strategy that offers the potential to create complex 3D objects from both synthetic and biological building blocks.[3,4] In this approach, a tightly focused, pulsed laser beam is scanned through a reagent solution, exciting a photosensitive species via non-resonant absorption of two or more photons within fabrication voxels often smaller than 1 fL. Activation of this reactive species in turn promotes radical-based solidification of reagents, allowing extended microforms to be fabricated with feature sizes as small as ≈100 nm.[5]

MPL primarily has been used to create 3D plastic microforms from synthetic resins.[5,6] Although remarkable from a morphological standpoint, such objects generally are impervious to solution and unresponsive to their local environment, and as a consequence, do not enjoy widespread use in applications requiring biological, chemical, and physical functionality (e.g., cell culture, actuation, chemical sensing).

To impart localized, definable functionality to 3D microstructures, several groups have investigated the use of biological molecules as reagents for MPL. A variety of soluble proteins, including bovine serum albumin (BSA), cytochrome c, avidin, and lysozyme, can be photocrosslinked to form (solid) 3D hydrogels,[7–12] materials characterized by high porosity and permeability,[13,14] tunable mechanical properties,[9] and a capacity to retain native activity of their molecular components.[12] In addition, it is possible to tailor the chemical functionality of protein-based hydrogels via conjugation to a diverse range of bioactive species and to trigger changes in microstructure size and shape using environmental cues,[13,15] attributes that have been exploited for 3D cellular organization[14,16] and microactuation.[13]

In principal, direct-write methods such as MPL can be used to fabricate any microscale 3D shape. Unfortunately, the need to prevent object drift[17] during and after fabrication has, in nearly all cases, required that materials be fabricated in integral contact with a stationary surface.[18,19] This requirement places substantial restrictions on the functionality and utility of possible microscale objects.

Although surface-adhered microforms may retain the capacity for internal motion (e.g., swelling and bending),[13] they lack the rotational and translational degrees of freedom necessary for many applications. Mechanical devices often employ components that retain a subset of degrees of freedom, objects that we classify here as partially constrained. A microscopic flywheel or gear, for example, must rotate about one axis (without translating),[20] while a piston translates in one dimension (without rotating).[6] Several research groups have previously reported MPL of partially constrained plastic microstructures (e.g., chain links, gears, paddlewheels) by allowing monomer solutions to evaporate into solid films that effectively eliminate object diffusion during fabrication.[6,21,22]

In other cases, desired functionality requires a microform to be fully unconstrained, retaining all rotational and translational degrees of freedom. Bulk preparation methods can be used to create objects of this class, but are useful primarily for producing

Dr. E. C. Spivey, Dr. E. T. Ritschdorff, J. L. Connell, C. A. McLennon, Prof. J. B. Shear
Department of Chemistry and Biochemistry
The University of Texas at Austin
Austin, TX 78712, USA
E-mail: jshear@mail.utexas.edu
Prof. C. E. Schmidt
Department of Biomedical Engineering
The University of Texas at Austin
Austin, TX 78712, USA

DOI: 10.1002/adfm.201201465

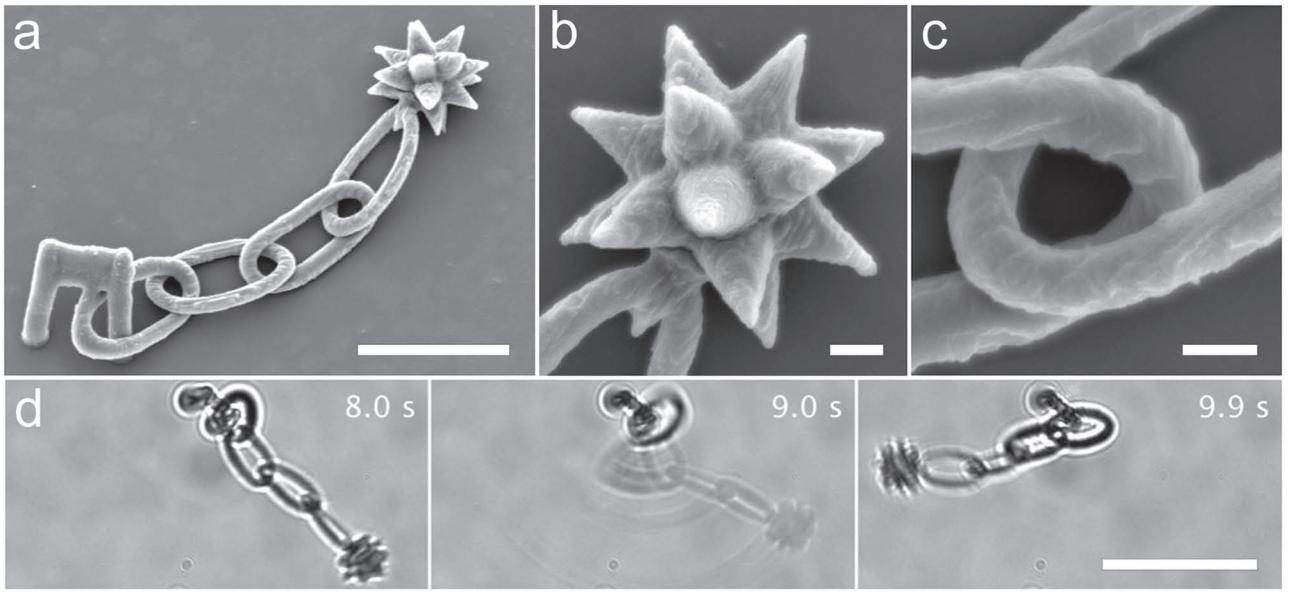

Figure 1. Multiphoton lithography (MPL) of a partially-constrained microstructure fabricated from a BSA protogel. a) Scanning electron microscopy (SEM) image of a BSA morningstar that contains four chain links and an 18-point spiked star. The morningstar is connected to the coverglass using a microfabricated clip. All elements (star, chain and clip) of the structure are fabricated using a single mask sequence. Scale bar, 20 µm. b) SEM image showing detail of the star. The radius of curvature of the points is ≈0.5 µm. Scale bar, 3 µm. c) SEM image showing detail of two interlocked morningstar chain links. Scale bar, 2 µm. d) Time-lapse bright-field sequence of the morningstar subjected to oscillatory flow. The chain freely responds to buffer convection, demonstrating that interlocked links are not fused. Images were extracted from Supporting Information Video 1; time stamp values correspond to the video. Scale bar, 30 µm.

spheroids and a limited range of additional geometries.[23,24] A few reports have described the use of MPL to fabricate simple unconstrained structures, including spheroids[25] and quasi-2D puzzle pieces,[26] objects that were subsequently manipulated using optical tweezers. Microparticles of complex, arbitrary shape would be of particular value in characterizing and tuning phagocytotic uptake (e.g., to optimize drug delivery)[27,28] and as tracers in microrheological studies.

Here, we report a strategy for creating a nearly unlimited range of microforms from crosslinked protein, including linked Möbius strips and nested cavities composed of multiple proteins, and describe MPL microfabrication of complex unconstrained objects. To avoid drift during fabrication of microforms that are not in integral contact with a surface, we developed a methodology for producing high-viscosity protein-based reagents (termed protogels) via controlled evaporation of a mixture of protein, photosensitizer, and DMSO in aqueous buffer. Protogels are prepared from a range of proteins and can be used to fabricate crosslinked microstructures with the capacity to retain native protein activity. We have exploited this lithographic strategy to fabricate complex cellular probes, including 18-point free-floating stars less than 10 µm tip-to-tip. Motile bacteria induce free rotation and translation of micro-stars via collisions and, indirectly, through the production of microscopic flow.

2. Results and Discussion

2.1. Design and Evaluation of Protogels

In our initial efforts to form protein-based reagents suitable for MPL of unconstrained microstructures, we attempted to fabricate protein gels via partial evaporation of high-concentration aqueous protein solutions under vacuum (initially, 30% (w/w) BSA, 5 mM rose bengal in a HEPES-buffered saline solution, pH 7.3). We found that the resultant gel-like material could be used to fabricate unconstrained, cross-linked protein structures via MPL. Unfortunately, the evaporative process was not reproducible, as the drying time needed to produce optically consistent gels appeared sensitive to small changes in protein concentration as well as ambient temperature and humidity. In cases where the reagent solution was over-dried, punctate microdomains formed within the gel, disrupting the integrity of fabricated microstructures.

Gel homogeneity improved dramatically by incorporating dimethyl sulfoxide (DMSO) in the BSA reagent solution. Both during formation of protogels and in their subsequent use, essentially no microdomains were observed for aqueous-DMSO protogels. For larger protogels (see Experimental Section for detailed protocol), weights of precursor solutions were compared to those of protogels after drying for 25 to 30 min. By making the approximation that changes in mass were caused by water loss alone (i.e., that no DMSO evaporates), final weight percentages of BSA and DMSO were calculated to be 40% ± 1% and 28% ± 1%, respectively ($n = 7$ protogels).

Protogels formed in this manner could be used to produce high-quality protein-based microforms, such as the morningstar shown in **Figure 1**. Fabrication of this structure (and other microforms in this report) was accomplished using a dynamic mask-based process previously described in detail in which 3D objects are represented as a series of images sequentially displayed on a digital micromirror device (DMD).[3] By raster-scanning a focused titanium:sapphire (Ti:S) laser beam across

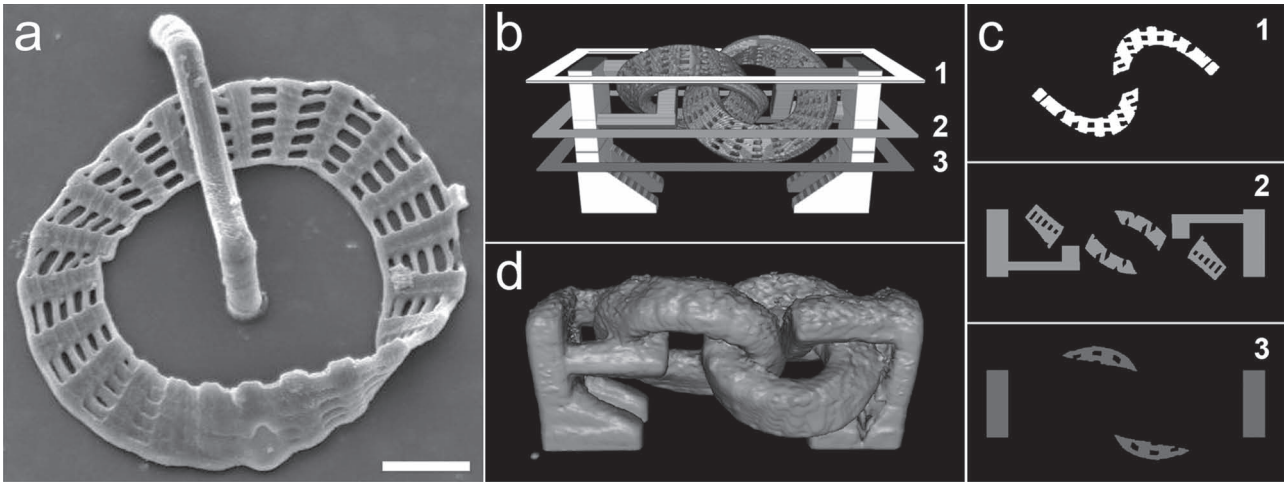

Figure 2. Protogel fabrication of non-adherent Möbius strips. a) SEM image of a single netted BSA Möbius strip, clipped to the coverglass surface by a staple-shaped retainer. Scale bar, 10 μm. b) Reconstruction of the mask sequence used to fabricate a two-link chain of netted Möbius strips in a top-down fashion. Individual masks, corresponding to planes identified with white, gray, and dark gray frames, are shown in detail in panel (c). d) 3D reconstruction of a stack of confocal images showing the isosurface of a BSA/bBSA structure functionalized with TMR-NAv. Few surface features of the Möbius strips are apparent in the isosurface presentation; however, more detail can be visualized in the raw confocal data (see Supporting Information Video 2). Isosurface represents a structure that is ≈75 μm wide and ≈30 μm tall.

the DMD, each mask directs fabrication in a single plane within the protogel, a process that is repeated as the focal plane within the reagent is incrementally shifted along the optical axis. To minimize distortions, nascent microforms must remain stationary during this process (a period of ≈3 min for the morningstar in Figure 1). We found that microstructures fabricated over periods of 15 min showed no evidence of distortions caused by drift within protogels.

The mechanisms by which DMSO assists formation of stable, homogeneous protogels have not been explored in detail, but multiple factors may be involved. When BSA is dissolved in pure aqueous solutions at concentrations higher than its calculated concentration in protogels, we found the viscosity to be insufficient for fabrication of un-anchored microstructures. The viscosity of binary water-DMSO mixtures previously has been shown to scale nonlinearly with DMSO content, with a maximum of ≈4 cP at ≈65% (w/w) DMSO.[29] Increases in viscosity from solvent alone, however, are minor compared to perturbations caused by 400 g L^{-1} BSA (η can be greater than 50 cP in aqueous solutions).[30] Of potentially more importance are changes in the characteristics of solvated proteins in aqueous-DMSO solvent systems, with a number of reports demonstrating increases in BSA hydrodynamic radius[31] and significant changes in viscosity for solutions of BSA in water-DMSO mixtures.[32] Moreover, vapor-pressure measurements on pure (binary) aqueous-DMSO mixtures have shown that the partial pressure of water decreases rapidly with increasing DMSO content,[33] a factor that may suppress evaporation.

2.2. Fabrication of Partially Constrained Structures

Links within the morningstar chain shown in Figure 1 have no direct connection to the glass substrate and are free to move individually, albeit with limitations on both translation and rotation imposed by adjacent links. As a consequence, this partially constrained object can swing under directional flow (Figure 1d and Supporting Information Video 1).

Figure 2 illustrates the capacity of dynamic-mask-based MPL to create protein-based microstructures of essentially unlimited complexity. In this example, "netted" BSA Möbius strips were retained both as individual objects (Figure 2a) and within chains (Figure 2d and Supporting Information Video 2). A 3D reconstruction of the masks used to fabricate the Möbius chain and three individual masks are shown in Figure 2b,c, respectively. Masks were displayed sequentially on the DMD in coordination with optical axis stepping of the sample stage. To avoid optical distortions that can occur when focusing through existing regions of a nascent structure, the Möbius chain was fabricated beginning ≈40 μm above the substrate with subsequent fabrication proceeding downward to the coverglass, a procedure that is not possible when using standard protein fabrication solutions. By subjecting the microstructure to oscillatory flow (Supporting Information Video 3), we confirmed that the interlocked Möbius links shown in Figure 2d were not fused. Similar structures also could be fabricated using lysozyme-based protogels (Supporting Information Figure 1).

To examine the possibility for creating functional micromechanical components using crosslinked protein, a 12-μm diameter paddlewheel was fabricated from a BSA protogel within a cylindrical chamber (**Figure 3** and Supporting Information Video 4). A vertical post, extending from the floor of the chamber to its ceiling, served to retain the paddlewheel. The cylinder wall contained a portal which provided entry to *Pseudomonas aeruginosa*, a rod-shaped motile bacterium ≈2 μm long and 0.5 μm wide that is propelled by a single flagellum. At a relatively low loading density (estimated to be ≈10 cells), the paddlewheel in Figure 3 can be observed rotating at a rate of ≈1 rpm.

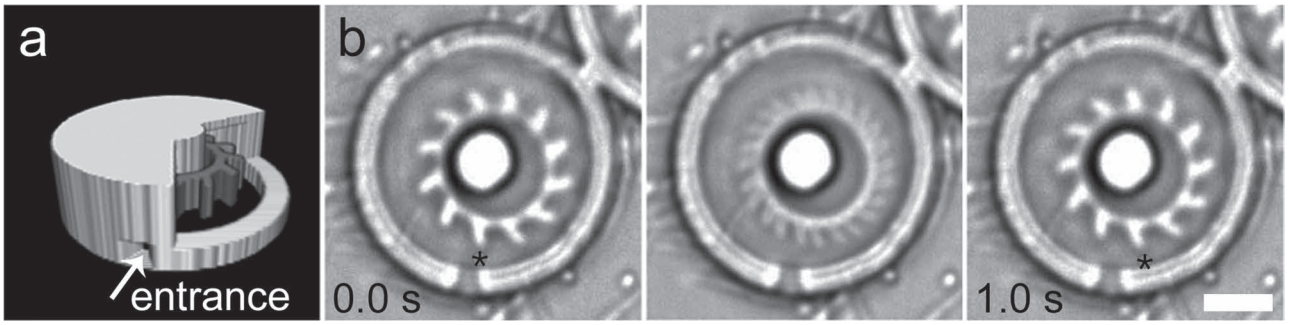

Figure 3. Actuation of a paddlewheel by motile bacteria. a) Cut-away of the reconstructed mask sequence used to fabricate partially constrained paddlewheels (dark gray) within cylindrical containers. b) Left and right panels: transmitted light images showing rotation of a BSA paddlewheel, driven by collisions with *Pseudomonas aeruginosa*, through an angle of ≈15° in a 1-s period (times correspond to those in Supporting Information Video 4). The paddlewheel is ≈3 μm thick and is contained in a housing ≈7 μm tall; a central post, extending from the floor to the ceiling of the housing, prevents the paddlewheel from being driven to the container wall. The black asterisk provides a point of reference to a specific paddle. Middle panel: Overlay of the left and right panels that shows rotation of the paddlewheel. Scale bar, 5 μm.

2.3. Protogels Made from Functional Proteins

Materials formed by multiphoton crosslinking of proteins are mechanically tunable, highly porous, and often biocompatible. In addition, the use of proteins in MPL offers great versatility in achieving desired bioactivity within 3D microstructures.[8,16] We have demonstrated previously that biotinylated BSA (bBSA) can be used to fabricate microstructures that display high avidin-binding capacity.[25] Such materials can be used to retain various biotinylated species, including enzymes, matrix proteins, and small molecules.[16,25] The Möbius chain, fabricated from a BSA protogel that contained some bBSA, was visualized using fluorescently tagged NeutrAvidin (Figure 2d).

It also is possible to directly incorporate proteins of desired activity into crosslinked matrixes, a more rapid, single-step strategy for creating functional materials that avoids steric limitations of avidin-sandwich protocols. Although various proteins have been shown to retain significant activity within matrixes fabricated from concentrated solutions (e.g., cytochrome c, glutamate dehydrogenase, avidin),[12,25] it was unclear whether the more severe physical and chemical environment within protogels would prohibitively compromise protein function.

To evaluate intrinsic activity in protogel-based microstructures, test structures were fabricated from avidin protogels (**Figure 4**a,b) and exposed to 24 μM fluorescein biotin. Avidin microstructures were found to bind four-fold greater labeled biotin than was retained by BSA control structures (Figure 4c). Specificity of this interaction was verified by blocking fluorescein biotin binding by pre-treating avidin microstructures with unlabeled biotin (Supporting Information Figure 2).

Although the structure shown in Figure 4 is fully constrained, it illustrates another advantage of protogel reagents: the capacity to fabricate objects with feature overhangs (i.e., regions unsupported by material directly below the feature). In conventional MPL using high-concentration protein solutions, plane-by-plane fabrication generally is not rapid enough to prevent drift of overhanging features. Although fabrication of the avidin structure is technically possible using a liquid precursor, use of protogel reagents significantly simplifies the process.

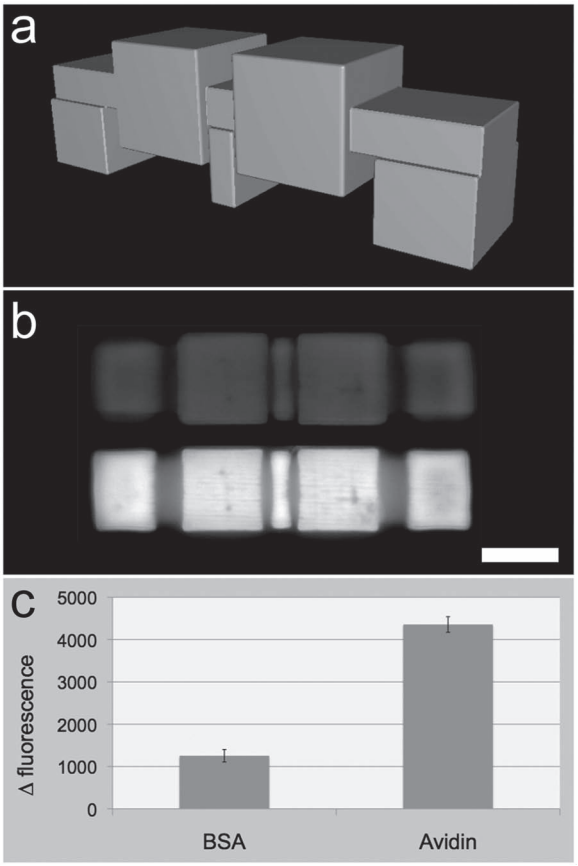

Figure 4. Microstructures fabricated from avidin protogels retain biotin-binding activity. a) 3D reconstruction of the mask sequence used to fabricate avidin and BSA microstructures. b) Wide-field fluorescence image of an avidin microstructure before and after fluorescein–biotin exposure and wash-out with HEPES buffer. The two central, square regions of each microstructure are faces of the unsupported cubes. Scale bar, 15 μm. c) Bar graph showing the change in fluorescence intensity of BSA and avidin microstructures before and after exposure to fluorescein biotin with HEPES buffer wash-out ($n = 4$). Error bars are $\pm 1\sigma$.

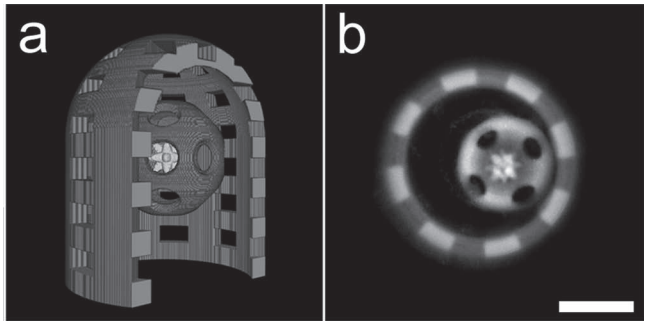

Figure 5. Multi-protein nested microstructure containing fully unconstrained objects. a) Cut-away of a 3D reconstruction of masks used to fabricate a nested structure in sequential steps from lysozyme and BSA protogels. A surface-attached lysozyme dome and unconstrained sphere were fabricated first (gray), followed by an unconstrained 18-point BSA star (light gray;placement of star mask was adjusted to accomodate settling of the sphere between steps). The dome is designed to be 60 μm tall and 50 μm in diameter, while the sphere is 29 μm in diameter; the star is designed to be 10 μm tip-to-tip. b) Integrated fluorescence from ten sequential confocal planes that intersected the lower half of the 18-point star. In this image, the star has settled to the bottom of the sphere. Images were acquired using emission from residual photosensitizer. Scale bar, 20 μm.

2.4. Nested Structures Containing Unconstrained Objects

Protogels could provide a means to create fully unconstrained microstructures of arbitrary geometry, objects of essentially any shape capable of translation and rotation without local constraint. To assess this possibility, we designed a complex nested structure in which a surface-adherent dome enclosed an unconstrained hollow sphere that, in turn, housed an unconstrained 18-point star (**Figure 5**). The dome and sphere were designed with rectangular and circular vent holes, respectively, to facilitate removal of un-crosslinked reagent and addition of subsequent solutions. Fabrication was performed in discrete steps in which the dome and sphere were crosslinked from a lysozyme protogel, and, following rehydration and reagent washout, a BSA protogel was formed and used to create the star.

As an initial platform for monitoring dynamic interactions between unconstrained objects and living cells, we designed traps to capture and retain motile bacteria within compartments containing a nested (unconstrained) probe. To promote facile entry of bacteria while minimizing cell escape, traps were designed with a funneled entry-way that guided swimming cells to a narrow pore, which opened into a hemispherical capture chamber (**Figure 6**a). In the center of the hemispherical chamber, we fabricated an unconstrained 18-point star with a spherical interior void.

Traps efficiently accumulated cells when incubated with *P. aeruginosa*. At moderate loading densities, the star was subjected to rapid buffeting, both from direct collisions with bacteria and by flagellum-generated convective flow. Figure 6b demonstrates the resultant free translation and rotation of the star in three dimensions (see also Supporting Information Video 5). Although a detailed microrheological analysis of the fluidic environment within the trap is beyond the scope of the current studies, such complex microprobes could provide insights into

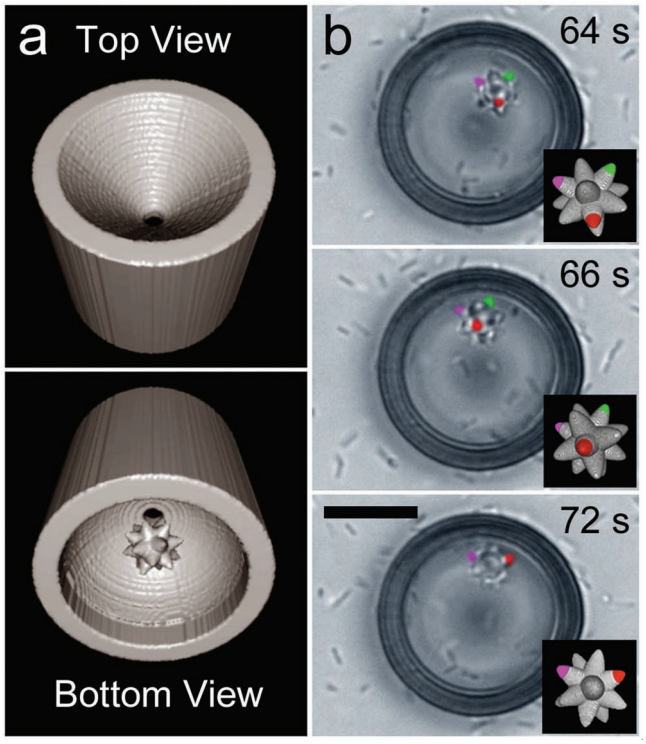

Figure 6. Probing bacterial motility using unconstrained microstructures. a) Reconstruction of the mask sequence used to fabricate bacterial traps containing unconstrained 18-point stars. The top frame shows the funneled surface used to guide bacteria toward a capture chamber containing a single unconstrained star. The bottom frame provides a view through the coverglass floor into the capture chamber, with a star positioned in the middle of a hemispherical chamber. b) Time sequence showing the tumbling movement of an 18-point BSA star caused by *P. aeruginosa* (time points are given relative to the start of Supporting Information Video 5). Insets (lower right corners) show representations of the star in the approximate orientations in each time-lapse frame. The cardinal axes of the stars are color coded for clarity. In the top frame (64.3 s), all cardinal axes of the star can be seen. By the middle frame (66.3 s), the star has rolled slightly, and translated several micrometers to its new position. Six seconds later, in the lower frame (72.6 s), the star has revolved so that the green reference point is hidden from view. No appreciable rotation or translation of stars is apparent in traps lacking bacteria. Scale bar, 15 μm.

fluid flow within defined populations of bacteria,[34,35] including those engaged in swarming motility.[36]

3. Conclusions

Complex protein-based microstructures that retain translational and rotational degrees of freedom represent a class of materials previously inaccessible to researchers. The technologies reported here offer a strategy for not only creating microscopic structures of essentially any imaginable shape, but for harnessing the attributes and functionality of biological materials within these objects. The versatility of protein-based micromaterials[10,13,37] provides opportunities for fabricating micromachines with tunable and spatially heterogeneous mechanical properties and environmental sensitivity, offering

greater flexibility, for example, in designing devices such as micro-pumps and rotors.[34,38] Moreover, the ability to localize chemical reactors to desired sub-components[12] should prove useful in exploiting chemistry to drive such devices. A complication in this application area arises from potential adhesion of microstructures to other objects in the environment. The current proof-of-concept studies did not investigate in detail the variables influencing attachment of protein-based materials, factors that may include molecular interactions, microstructure geometry and local buffer flow. We are confident that a systematic evaluation of attachment will identify approaches to mitigate unwanted interaction of microobjects (e.g., addition of passivating agents, adjustment of pH).

Protein-based microparticles could prove useful in drug delivery, where recent studies have indicated that macrophage clearing of microscale particles via phagocytosis may be critically dependent on the object's size and shape.[27] Currently, micro- and nanoscale hydrogels are limited to spheroids or simple geometric shapes including disks and pyramids.[23,24] By systematically assessing cellular interactions with a much broader range of microparticle shapes, it may be feasible to tune drug-delivery vehicles to either minimize removal of drugs by macrophages, or, alternately, to target delivery to these cells (for example, in the case of diseases residing in or enabled by macrophages).[27,28]

The use of protogels as a reagent for MPL greatly extends the geometric possibilities for biological micro-objects, and as such, opens opportunities for a range of novel tools, especially in the area of biomedical research. We anticipate that these materials will be rapidly integrated into strategies to control and assess cellular microenvironments.

4. Experimental Section

Instrumentation and Setup: The dynamic-mask MPL instrumentation used in this study is based on the strategy described in detail by Nielson et al.[3] and modified by Ritschdorff et al.[39] Briefly, the collimated output beam of a mode-locked Ti:sapphire laser tuned to 740 nm (Coherent Mira 900F) was focused onto a two-axis, galvanometer-driven scan mirror, with scan waveforms, frequencies, amplitudes, and phases controlled by software written in-house using LabVIEW. The scanned beam was directed through a series of relay lenses and focused onto 800 × 600 (SVGA) DMD (from a partially dismantled DLP projector; BenQ, MP510), which modulated the beam intensity according to binary mask images. At mask positions representing "positive" fabrication pixels, the beam was reflected from the DMD at ≈20° relative to the normal, collimated using a tube lens, and directed by a dichroic mirror into an infinity-corrected 100×, 1.3 NA Zeiss Fluar microscope objective. In this manner, the fabrication plane was positioned at a plane conjugate to the DMD, providing the means to direct protein photocrosslinking at specific planes within the protogel according to patterns displayed on the mask. Because the tube lens/microscope objective combination provided an approximate 100-fold optical reduction, eight (linear) pixels in the mask corresponded to ≈1 μm within the fabrication plane.

Protogel Preparation: HEPES buffer was prepared from 20 mM (pH 7.3) HEPES (L6876, Sigma-Aldrich, St. Louis, MO) and 100 mM NaCl. Stock solutions of photosensitizer (50 mM eosin Y [201930250, Acros Organics, Geel, Belgium] or 15 mM methylene blue (M9140, Sigma-Aldrich)) were prepared in DMSO and diluted by a factor of 3.5 in HEPES buffer. Lyophilized BSA (BAH-64, Equitech-Bio, Kerrville, TX), avidin (A887, Invitrogen, Carlsbad, CA) or lysozyme (L6876, Sigma-Aldrich) was then added dry to the photosensitizer solution, yielding final weight percentages of 29% and 21% for protein and DMSO, respectively. The protogels used to fabricate the microstructures in Figure 4 were made from a solution containing eosin Y; all other protogels were made from solutions containing methylene blue. Samples were left on a rotating mixer for up to 12 h at ≈20 °C to ensure complete dissolution of the protein. Some BSA hydrogels were made using a precursor solution in which ≈20% of the BSA was biotinylated, providing the ability to fabricate avidin-binding BSA microstructures. bBSA was prepared from BSA and biotin-succinimidyl ester (M0785, Marker Gene Technologies Inc., Eugene, OR) using standard protocols from the manufacturer.

Wells for precursor solution were constructed by placing PDMS rings on glass coverslips. Two different sized wells were constructed using ≈1-mm-thick rings of cured PDMS with either 4- or 6-mm-diameter center holes. PDMS rings were cleaned thoroughly using detergent, rinsed, then oven dried at ≈60 °C and allowed to adhere to #1 thickness (24 mm x 60 mm) cover glass. Wells were filled with precursor solution to a level such that the surface was slightly convex, placed into a drying chamber (Supporting Information Figure 3) and subjected to a flow of dry nitrogen (≈20 mL s^{-1}) for either ≈15 min (4-mm holes) or ≈25 min (6-mm holes). In some cases, BSA precursor solutions were weighed before drying and compared with the initial mass of the resultant BSA protogel. After drying, wells containing the protogel were covered with 1-cm-diameter circular cover glass to inhibit additional drying.

Fabrication of Protein Microstructures: Laser power was adjusted using a half-wave-plate/polarizer pair to 15–25 mW, measured at the back aperture of the microscope objective. Raster scanning provided a fast-axis scan velocity of ≈7 mm s^{-1} and a slow-axis velocity of ≈6 μm s^{-1}, values selected so that lines of crosslinked protein overlapped to produce a continuous plane. Both the raster scan and optical axis movements were controlled and coordinated by a PC via a program written in LabVIEW (v. 8.2, National Instruments, Austin, TX).

Masks typically were produced using ImageJ macro language (http://rsbweb.nih.gov/ij/developer/macro/macros.html; ImageJ v1.44o, by Wayne Rasband, NIH, Bethesda, MD). Fabrication of 3D microstructures was accomplished by displaying a series of mask images in which each image directed a corresponding cross section of the desired structure. Movement of the protogel along the optical axis was performed using a three-axis translational stage (model 562, Newport Corp., Irvine, CA) driven by motorized actuators (model LTA-HS and model ESP300 motion controller/driver, Newport Corp., Irvine, CA). Movements were incremented in 0.33- or 0.50-μm steps.

Rehydration of protogels was accomplished by applying 50 μL of HEPES buffer to the exposed surface of the protogel. After incubation for 10 min at ≈20 °C, the rehydrated protogel was removed using a micropipette, and the structures were rinsed with ten 50-μL volumes of HEPES buffer.

Microstructures fabricated from protogels containing bBSA were incubated in HEPES buffer-filled wells for ≥12 h under ambient conditions (≈20 °C) to reduce fluorescence caused by residual photosensitizer, then incubated with 20 μg/mL tetramethylrhodamine-NeutrAvidin (A6373, Invitrogen) or Oregon Green-NeutrAvidin (A6374, Invitrogen) in HEPES buffer for ≥12 h. Structures were rinsed ten times by filling wells completely with HEPES buffer, then incubated for an additional ≈12 h in HEPES buffer before imaging.

In the two-stage protogel fabrication shown in Figure 5, a BSA/bBSA solution was applied to existing lysozyme structures for 30 min before controlled drying to ensure that the solution had reached the interior of the dome and sphere. Although incorporation of bBSA can provide a means to selectively label a subset of crosslinked objects with biotinylated ligands,[16] we observed high non-specific adsorption of bBSA to pre-existing lysozyme domes and spheres, a finding consistent with the large difference in lysozyme and BSA isoelectric values.

Biotin-Binding Measurements: Microstructures fabricated from avidin protogels were incubated in HEPES buffer-filled wells for 24 h (≈20 °C), then incubated with fluorescein biotin (24 μM; B1370, Invitrogen) or biocytin tetramethylrhodamine (biocytin TMR, 23 μM; T12921, Invitrogen) in HEPES buffer for 24 h. Structures then were rinsed with ten well volumes of HEPES buffer and incubated for an additional 24 h before imaging. In biotin-blocking studies, square avidin pads were pre-incubated with biotin (1.0 mM; B1595, Invitrogen) for 24 h

before incubation with biocytin TMR. Relative biotin-binding by avidin and control (BSA) microstructures was quantified within equal-area sub-regions on elevated cubes or pads.

Image Acquisition: Bright-field and wide-field fluorescence images of microstructures were acquired using a Zeiss Axiovert 135 inverted microscope with a 40×, 0.75 NA objective. For fluorescence images, we used the attached Zeiss HBO-100 mercury arc lamp and standard FITC and CY3/TRITC filter sets (49011 and 49004, respectively, Chroma Technology, Rockingham, VT).

Confocal image stacks were acquired using a Leica SP2 AOBS confocal microscope and either a 63×, 1.4 NA oil objective, or a 63×, 1.3 NA water objective. Step sizes between confocal planes were selected based on the minimum expected feature size along the optical axis, and ranged from 0.1–1.0 µm. All images were processed using ImageJ software. Volume and isosurface 3D representations of confocal stacks and mask stacks were constructed using the "3D viewer" plugin (open source code, written by Benjamin Schmid). The image in Figure 5b represents integration of ten sequential planes (from the rhodamine channel) spanning a 2.9-µm section intersecting the lower half of the 18-point star.

Scanning Electron Microscopy: Electron microscopy images were acquired using an FEI Quanta 650 FEG environmental scanning electron microscope (ESEM) in high vacuum mode. Protein microstructures were prepared for the SEM by soaking in HEPES buffer at ≈20 °C for 24 h, followed by 15 min incubation in 5% (v/v) glutaraldehyde (18426, Ted Pella, Inc., Redding, CA) to enhance protein crosslinking. Microstructures then were gradually dehydrated via sequential washes with deionized water, a 1:1 mixture of ethanol and deionized water, ethanol, a 1:1 mixture of ethanol and methanol, and methanol (each wash lasting 15 min). After the final wash, protein microstructures were placed in a drying oven at 70 °C for 15 min, then in a dessicator for 3 h, and finally sputter coated to a nominal thickness of 20 nm with Pt-Pd alloy using a Cressington 208 benchtop sputter coater.

Bacterial Cell Culture: *P. aeruginosa* PA01 carrying the pMRP9-1 gfp plasmid was grown to saturation aerobically at 37 °C overnight in tryptic soy broth (TSB) containing 300 mg mL^{-1} carbenicillin (for plasmid maintenance). An aliquot from the culture then was diluted and grown to mid-exponential phase. *P. aeruginosa* cells in TSB were introduced into 2 mL wells containing protein microstructures. Interactions between the cells and microstructures were observed and recorded over periods of up to 8 h at ≈20 °C.

Supporting Information

Supporting Information is available from the Wiley Online Library or from the author.

Acknowledgements

The authors gratefully acknowledge support from an NSF CBET grant (0829166), the Welch Foundation (F-1331), the Sam Y. Zamrik Endowed Fellowship in Engineering at the University of Texas at Austin Cockrell School of Engineering (awarded to E.C.S.), and the U.S. Department of Veteran's Affairs VEAA grant (awarded to E.C.S.). The authors thank Tim Hooper for assistance with the laser scanner and DMD instrumentation.

Received: May 31, 2012
Published online: August 24, 2012

[1] M. D. Huntington, T. W. Odom, *Small* **2011**, *7*, 3144.
[2] M. Caldorera-Moore, M. K. Kang, Z. Moore, V. Singh, S. V. Sreenivasan, L. Shi, R. Huang, K. Roy, *Soft Matter* **2011**, *7*, 2879.
[3] R. Nielson, B. Kaehr, J. B. Shear, *Small* **2009**, *5*, 120.
[4] S. Maruo, A. Takaura, Y. Saito, *Opt. Express* **2009**, *17*, 18525.
[5] S. Maruo, O. Nakamura, S. Kawata, *Opt. Lett.* **1997**, *22*, 132.
[6] S. M. Kuebler, M. Rumi, T. Watanabe, K. Braun, B. H. Cumpston, A. A. Heikal, L. L. Erskine, S. Thayumanavan, S. Barlow, S. R. Marder, J. W. Perry, *J. Photopolym. Sci. Technol.* **2001**, *14*, 657.
[7] J. Pitts, A. Howell, R. Taboada, I. Banerjee, J. Wang, S. Goodman, P. Campagnola, *Photochem. Photobiol.* **2002**, *76*, 135.
[8] B. Kaehr, R. Allen, D. J. Javier, J. Currie, J. B. Shear, *Proc. Natl. Acad. Sci. USA* **2004**, *101*, 16104.
[9] C. Y. Khripin, C. J. Brinker, B. Kaehr, *Soft Matter* **2010**, *6*, 2842.
[10] Y. L. Sun, W. F. Dong, R. Z. Yang, X. Meng, L. Zhang, Q. D. Chen, H. B. Sun, *Angew. Chem. Int. Ed.* **2012**, *51*, 1558.
[11] F. Dawood, S. Qin, L. Li, E. Y. Lin, J. T. Fourkas, *Chem. Sci.* **2012**, *3*, 2449.
[12] R. T. Hill, J. B. Shear, *Anal. Chem.* **2006**, *78*, 7022.
[13] B. Kaehr, J. B. Shear, *Proc. Natl. Acad. Sci. USA* **2008**, *105*, 8850.
[14] J. L. Connell, A. K. Wessel, M. R. Parsek, A. D. Ellington, M. Whiteley, J. B. Shear, *mBio* **2010**, *1*, e00202.
[15] J. R. Khurma, D. R. Rohindra, A. V. Nand, *Polym. Bull.* **2005**, *54*, 195.
[16] S. K. Seidlits, C. E. Schmidt, J. B. Shear, *Adv. Funct. Mater.* **2009**, *19*, 3543.
[17] B. Kaehr, N. Ertas, R. Nielson, R. Allen, R. T. Hill, M. Plenert, J. B. Shear, *Anal. Chem.* **2006**, *78*, 3198.
[18] S. Basu, P. J. Campagnola, *J. Biomed. Mater. Res. B* **2004**, *71*, 359.
[19] T. Baldacchini, C. N. LaFratta, R. A. Farrer, M. C. Teich, B. E. A. Saleh, M. J. Naughton, J. T. Fourkas, *J. Appl. Phys.* **2004**, *95*, 6072.
[20] S. Maruo, K. Ikuta, H. Korogi, *J. Microelectromech. Sys.* **2003**, *12*, 533.
[21] D. Wu, Q.-D. Chen, L.-G. Niu, J.-N. Wang, J. Wang, R. Wang, H. Xia, H.-B. Sun, *Lab Chip* **2009**, *9*, 2391.
[22] T. Sawada, Y. Hiratsuka, M. Miyata, S. Maruo, *15th Int. Conf. Miniaturized Sys. Chem. Life Sci*. RSC Publishing, **2011**, 1849.
[23] D. Dendukuri, K. Tsoi, T. A. Hatton, P. S. Doyle, *Langmuir* **2005**, *21*, 2113.
[24] J. A. Champion, Y. K. Katare, S. Mitragotri, *Proc. Natl. Acad. Sci. USA* **2007**, *104*, 11901.
[25] R. Allen, R. Nielson, D. D. Wise, J. B. Shear, *Anal. Chem.* **2005**, *77*, 5089.
[26] P. J. Rodrigo, L. Kelemen, C. A. Alonzo, I. R. Perch-Nielsen, J. S. Dam, P. Ormos, J. Glückstad, *Opt. Express* **2009**, *15*, 9009.
[27] G. Sharma, D. T. Valenta, Y. Altman, S. Harvey, H. Xie, S. Mitragotri, J. W. Smith, *J. Controlled Release* **2010**, *147*, 408.
[28] S. Venkataraman, J. L. Hedrick, Z. Y. Ong, C. Yang, P. L. R. Ee, P. T. Hammond, Y. Y. Yang, *Adv. Drug Delivery Rev.* **2011**, *63*, 1228.
[29] R. G. LeBel, D. A. I. Goring, *J. Chem. Eng. Data* **1962**, *7*, 100.
[30] W. Du, A. M. Klibanov, *Biotechnol. Bioeng.* **2011**, *108*, 632.
[31] A. Huang, C. Liu, L. Ma, Z. Tong, R. Lin, *J. Chem. Thermodyn.* **2012**, *49*, 95.
[32] S. G. Elfbaum, K. Laden, *J. Soc. Cosmetic Chem.* **1968**, *19*, 163.
[33] X. Q. Qian, B. X. Han, Y. Liu, H. K. Yan, R. L. Liu, *J. Solution Chem.* **1995**, *24*, 1183.
[34] A. Sokolov, M. M. Apodaca, B. A. Grzybowski, I. S. Aranson, *Proc. Natl. Acad. Sci. USA* **2010**, *107*, 969.
[35] B. Behkam, M. Sitti, *2007 7th IEEE Conf. Nanotechnol.* **2007**, *Vol 1–3*, 727.
[36] N. C. Darnton, L. Turner, S. Rojevsky, H. C. Berg, *Biophys. J.* **2010**, *98*, 2082.
[37] J. W. Nichol, S. T. Koshy, H. Bae, C. M. Hwang, S. Yamanlar, A. Khademhosseini, *Biomaterials* **2010**, *31*, 5536.
[38] M. J. Kim, K. S. Breuer, *Small* **2008**, *4*, 111.
[39] E. T. Ritschdorff, R. Nielson, J. B. Shear, *Lab Chip* **2012**, *12*, 867.